Journal of Medical Radiation Sciences

Open Access

ORIGINAL ARTICLE

An investigation into the effect of changing the computed tomography slice reconstruction interval on the spatial replication accuracy of three-dimensional printed anatomical models constructed by fused deposition modelling

Ben Searle, BMedImg (Honours),[1,2] & Deborah Starkey, MAppSc, MEd, FIR, SFHEA[2]

[1]Redcliffe Hospital, Redcliffe, QLD, Australia
[2]School of Clinical Sciences, Faculty of Health, Queensland University of Technology, Brisbane, QLD, Australia

Keywords
3D-printing, computed tomography, fused deposition modelling, biofabrication, slice reconstruction interval

Correspondence
Benjamin Searle, School of Clinical Sciences, Faculty of Health, Queensland University of Technology, Queensland, Australia. Tel: +61401175483; Fax: +6173138152; Email: searle.j.benjamin@gmail.com

Received: 6 September 2019; Revised: 7 January 2020; Accepted: 7 January 2020

J Med Radiat Sci **67** (2020) 43–53

doi: 10.1002/jmrs.382

Abstract

Introduction: Three-dimensional (3D) printed models can be constructed utilising computed tomography (CT) data. This project aimed to determine the effect of changing the slice reconstruction interval (SRI) on the spatial replication accuracy of 3D-printed anatomical models constructed by fused deposition modelling (FDM). **Methods:** Three bovine vertebrae and an imaging phantom were imaged using a CT scanner. The Queensland State Government's *Animal Care and Protection Act 2001* did not apply as no animals were harmed to carry out scientific activity. The data were reconstructed into SRIs of 0.1, 0.3, 0.5 and 1 mm and processed by software before 3D printing. Specimens and printed models were measured with calipers to calculate mean absolute error prior to statistical analysis. **Results:** Mean absolute error from the original models for the 0.1, 0.3, 0.5 and 1 mm 3D-printed models was 0.592 ± 0.396 mm, 0.598 ± 0.479 mm, 0.712 ± 0.498 mm and 0.933 ± 0.457 mm, respectively. Paired t-tests ($P < 0.05$) indicated a statistically significant difference between all original specimens and corresponding 3D-printed models except the 0.1 mm vertebrae 2 ($P = 0.061$), 0.3 mm phantom 1 ($P = 0.209$) and 0.3 mm vertebrae 2 ($P = 0.097$). **Conclusion:** This study demonstrated that changing the SRI influences the spatial replication accuracy of 3D-printed models constructed by FDM. Matching the SRI to the primary spatial resolution limiting factor of acquisition slice width or printer capabilities optimises replication accuracy.

Introduction

The use of three-dimensional (3D) printing in medicine is expanding rapidly. Scan data can be printed by 3D printers to create replicas of anatomy that can be held, manipulated, studied and utilised in surgical planning, medical training and patient education.[1–5] Previously, clinical training and education of health practitioners has relied on the use of human cadavers.[6] Difficulties reported from this approach include the lack of patient-specific pathological representation and inconsistencies within unique human anatomy.[7,8] However, the use of models provides realistic and low-cost alternatives, particularly where financial limitations or cultural considerations impede use.[6] Now, clinicians can produce 3D models from patient scan data to improve the diagnosis, visualisation and management of pathology, whilst surgeons may plan and rehearse difficult surgical approaches prior to performing intraoperative surgery.[1,3,4,7] Clinicians can create guides that follow a patient's unique anatomy or fabricate lattice structures on medical implants to promote osseointegration and reduce risk of rejection.[1,3,5,7] Models can be used to educate patients and their families about an upcoming surgery or to communicate the surgical steps to a clinical team.[5] Finally, this technology can be utilised to create tissue-

equivalent anthropomorphic phantoms to refine computed tomography (CT) scan protocols.[2,9]

Reported benefits of the implementation of medical model use in surgery include an operating room time reduction of 10–20% in a range of clinical scenarios.[10,11] However, inaccurate anatomical representation is a reported flaw in these surgical applications, which can lead to suboptimal treatment planning.[5,10,11] For example, George et al.[10] reported examples of model defects including occluded foramina, blurred sutures or vascular models that eliminate arteries visible in CT angiograms.

The production of 3D-printed models can be summarised in four discrete steps as illustrated in Figure 1:

1. Acquisition of the scan data utilising imaging technology.
2. Segmentation of the scan data to isolate anatomy of interest.
3. Triangulation of scan data by translating image voxels into a mesh surface composed of triangular patches that encloses those voxels.
4. 3D printing to create the model.

Fused deposition modelling (FDM) is a 3D printing technology particularly relevant in medical applications. FDM is well suited to medical applications due to accessibility and reduced expense.[10] FDM printers can be operated and maintained without advanced training and can easily fit into existing workspaces.[12,13] In the FDM process, filaments are melted through a nozzle to a bed whilst cooling and solidifying during extrusion. Successive layers are deposited to create 3D replications of the relevant medical imaging file.[14] Typically, FDM cannot print features less than 0.3 mm in any dimension accurately due to nozzle width limitations, serving as a primary limitation to replication accuracy from a printing perspective.[10]

CT scanners are the gold standard for imaging bony anatomy due to superior hard tissue contrast and spatial resolution.[3–5] CT allows the segmentation of anatomy by utilising the Hounsfield values of the voxels in the scan data set.[13] The Hounsfield values of tissues reflect their attenuation of X-ray and are proportional to their physical density, for example, bone has a significantly higher Hounsfield value compared to soft tissue.[4] Segmentation can isolate bone from soft tissue to produce 3D replicas of bony structures or separate contrast-filled vascular structures from neighbouring anatomy to model aneurisms.[13] Segmentation may be automatic (dependent on Hounsfield values of voxels), manual (operator-defined spatial selection) or semi-automatic (combination of both).[3,5,10,14]

In a single-detector CT scanner, the slice width is limited by detector size and the collimation of the X-ray beam along the *z*-axis.[15] In multi-detector CT scanners, the slice width is determined by the detector element dimensions along the z-axis.[15] The minimum acquisition slice width is defined by the minimum detector width. Slice width has a direct impact on 3D models created from an imaging data set, as higher slice widths result in lower image resolution and anatomical detail.[8] The data from consecutive detector elements in a CT scanner can be combined to reconstruct a number of image series at a range of slice widths from the same raw scan data.[15] This is determined by the slice reconstruction interval (SRI), which represents the distance between the centre of adjacent slices in scan data. Decreasing the SRI can improve the visualisation of abnormal anatomy that may otherwise be concealed by volume averaging and minimise stair-step artefacts, but at the expense of larger data sets.[16,17] From an imaging perspective, slice thickness and SRI have been identified by Winder and Bibb (2005, cited by van Eijnatten et al.)[5] as primary limiting factors for the overall replication accuracy of 3D-printed models. This is supported by Huotilainen et al.[18] who found 3D printers are generally capable of printing with spatial resolution better than the slice thicknesses of most clinical CT scanners.

Due to the novel nature of the technology, there is a lack of published literature addressing the influence of reconstruction in CT scan data on the accurate

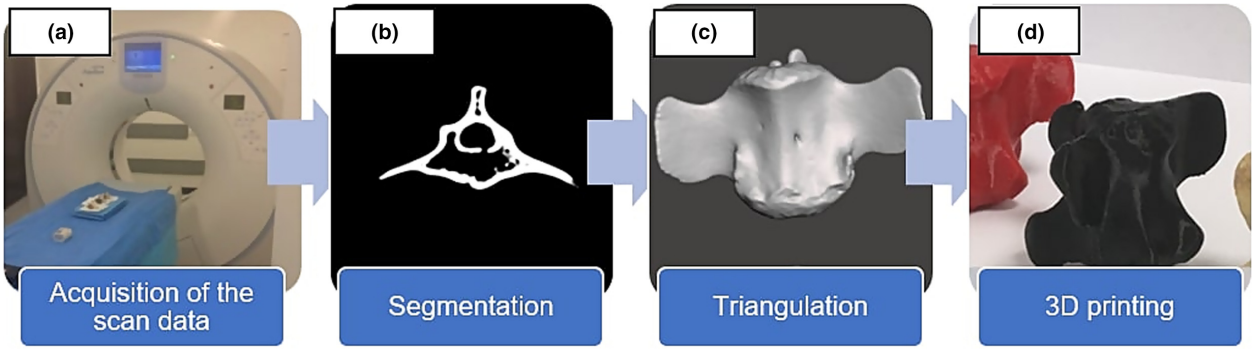

Figure 1. Scan-to-print 3D printing pipeline.

reproduction of 3D-printed anatomical models, particularly the SRI. McMenamin et al.[6], Odeh et al.[1], Allan et al.[9] and Bortolotto et al.[13] measured replication accuracy in pilot studies that evaluated the emerging technology. Van Eijnatten et al.[5] evaluated the influence of varying CT image segmentation methods in 3D printing, whilst Primo et al.[16] assessed replication accuracy differences between multislice CT and cone-beam CT. Petropolis et al.[12] evaluated the influence of changing printer layer height on spatial replication accuracy whilst Salmi et al.[19] analysed replication accuracy variances between selective layer sintering, 3D-printing and PolyJet printing technologies. Ogden et al.[20] evaluated the impact of different reconstruction kernels on the accuracy of 3D-printed models. No literature addressed the influence of the SRI on replication accuracy. This provides significant rationale to evaluate the influence of changing the SRI on model replication accuracy, particularly where complications may be avoided by refining this technology.[9]

This project aimed to determine if changing the slice reconstruction interval in CT scan data influences the spatial replication accuracy of 3D-printed anatomy constructed by fused deposition modelling and to determine if there may be a benefit in this process.

Methods

Three bovine coccygeal vertebrae (Fig. 2) and a European Forearm Phantom (Quality Assurance in Radiology and Medicine, GmbH, Möhrendorf, Germany) (Fig. 3) were scanned utilising a 16 slice CT scanner (Toshiba Aquilion Lightning, Toshiba American Medical Systems Inc., Tustin, CA, USA) at Queensland University of Technology's Medical Engineering Research Facility. The phantom, which contains two bone-equivalent solid materials encased in water-equivalent resin, is used to test peripheral bone densitometry systems. The 'Principles of Laboratory Animal Care' (NIH Publication Vol 25, No. 28 revised 1996; https://grants.nih.gov/grants/olaw/guide-for-the-care-and-use-of-laboratory-animals.pdf) were followed. There is no national Australian legislation applying to animal welfare in research. The Queensland State Government's *Animal Care and Protection Act 2001* did not apply to the bovine vertebrae as the animals were not killed for the purpose of carrying out a scientific activity.[21] The specimens were positioned in line and imaged separately. Each acquisition was acquired with 120 kV and 150 mAs, a 0.5 mm slice width and a 180 mm field of view. These parameters were selected to align to parameters commonly used in clinical practice, using the minimal slice width possible to maintain maximal resolution and detail.[13,16] The scan data were reconstructed into SRIs of 0.1, 0.3, 0.5 and 1 mm, using a soft tissue standard reconstruction algorithm.

Standardised processing was used for all image sets. The CT data output was a Digital Imaging and Communications in Medicine (DICOM) file of each original specimen. Each DICOM file was imported into 3D Slicer version 4.8 (The Slicer Community, Harvard, MA, USA), an open-source software package for medical imaging computing.[22] A segmented model was created for each DICOM file, utilising a threshold of 130 Hounsfield units to remove surrounding foam support and the water-equivalent resin surrounding the phantom (Fig. 4).

High-resolution surface extraction was performed to create a triangulated stereolithography (STL) mesh file, which was imported into Meshmixer version 3.5 (Autodesk inc., San Rafael, CA, USA).[23] The automated analysis function was used to inspect the mesh and repair faults that may contribute to print errors (Fig. 5). The file was exported to a Malyan M200 3D printer (Zhangzhou Changfeng Computer Equipment Co., Ltd, China) for assembly before support structures were removed (Fig. 6). The printer used in the study has a x-y resolution of 0.011 mm, layer resolution of 0.1 mm and a nozzle width of 0.4 mm.

Measurements were taken of anatomical features from both the original vertebrae and 3D-printed models concurrently using Kincrome K11100 digital calipers (Kincrome Australia Pty Ltd, Scoresby, Victoria, Australia), which has an accuracy of measurement of

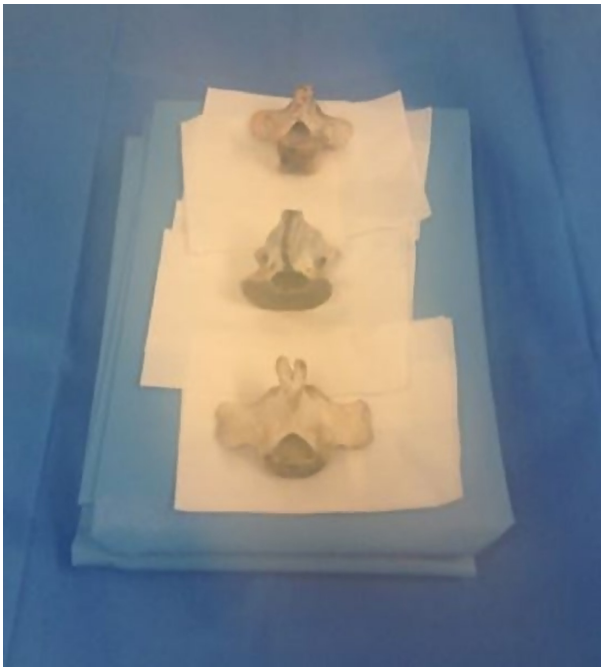

Figure 2. Bovine coccygeal vertebrae.

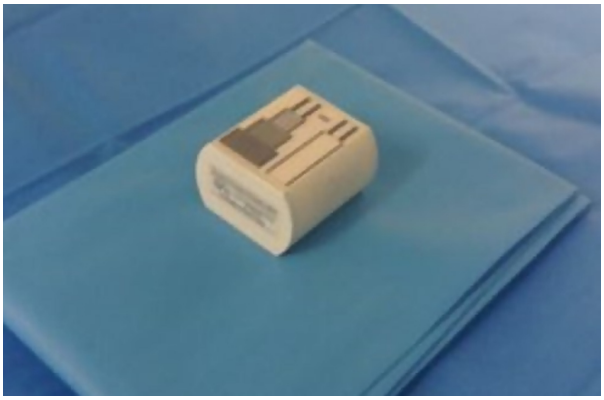

Figure 3. European forearm phantom (Quality assurance in radiology and medicine, GmbH, Möhrendorf, Germany).

±0.01 mm. Measurements were noted from the phantom model manual. Absolute error was calculated as the absolute difference (mm) between each original specimen measurement and the corresponding 3D-printed model measurement. The per cent relative error was calculated as the absolute difference divided by the original specimen measurement, multiplied by 100. The data were analysed using SPSS version 25 (IBM Corp., Armonk, NY, USA), where comparisons of the original specimens and the 3D-printed models were made using paired t-tests, with the level of significance set at $P < 0.05$. The intraclass correlation coefficient (ICC) was calculated to assess how strongly the data from the original specimens and corresponding 3D-printed models resembled each other.

Corresponding linear measurements were taken of each virtual 3D model in Meshmixer.

Results

3D-printing of the scanned specimens produced highly realistic 3D replicas that were suitable for measurement and analysis. The linear measurements of anatomical features of the original specimens and 3D-printed models are summarised in Table 1. Measurements ranged from 4.97 to 69.86 mm. Digital linear measurements obtained in Meshmixer of each virtual 3D model are displayed in Table 2.

Absolute error and per cent relative error of the linear measurements of the original specimens and 3D-printed models are summarised in Table 3. Absolute error ranged from 0 to 1.91 mm. Increasing the SRI was shown to increase the mean absolute error between comparative

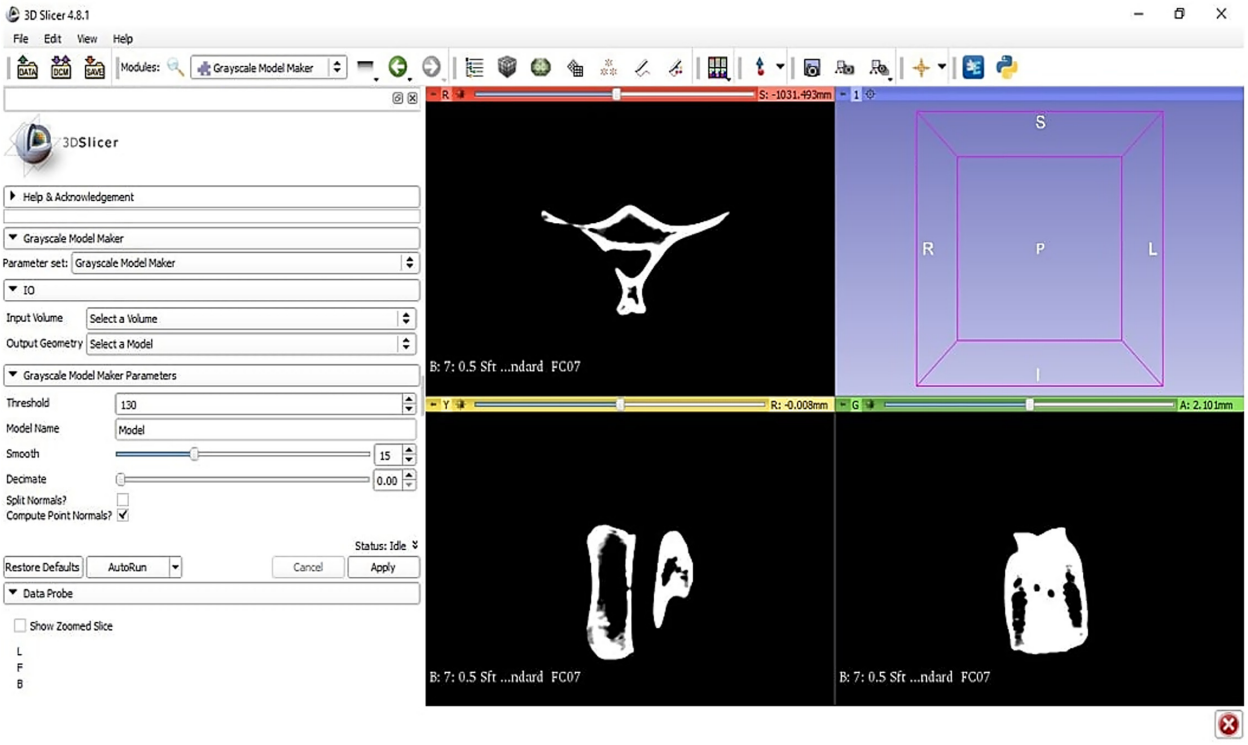

Figure 4. Segmentation and triangulation of the bovine vertebrae in 3D slicer version 4.8 (The Slicer Community, Harvard, MA, USA), an open-source software package for medical imaging computing.[22]

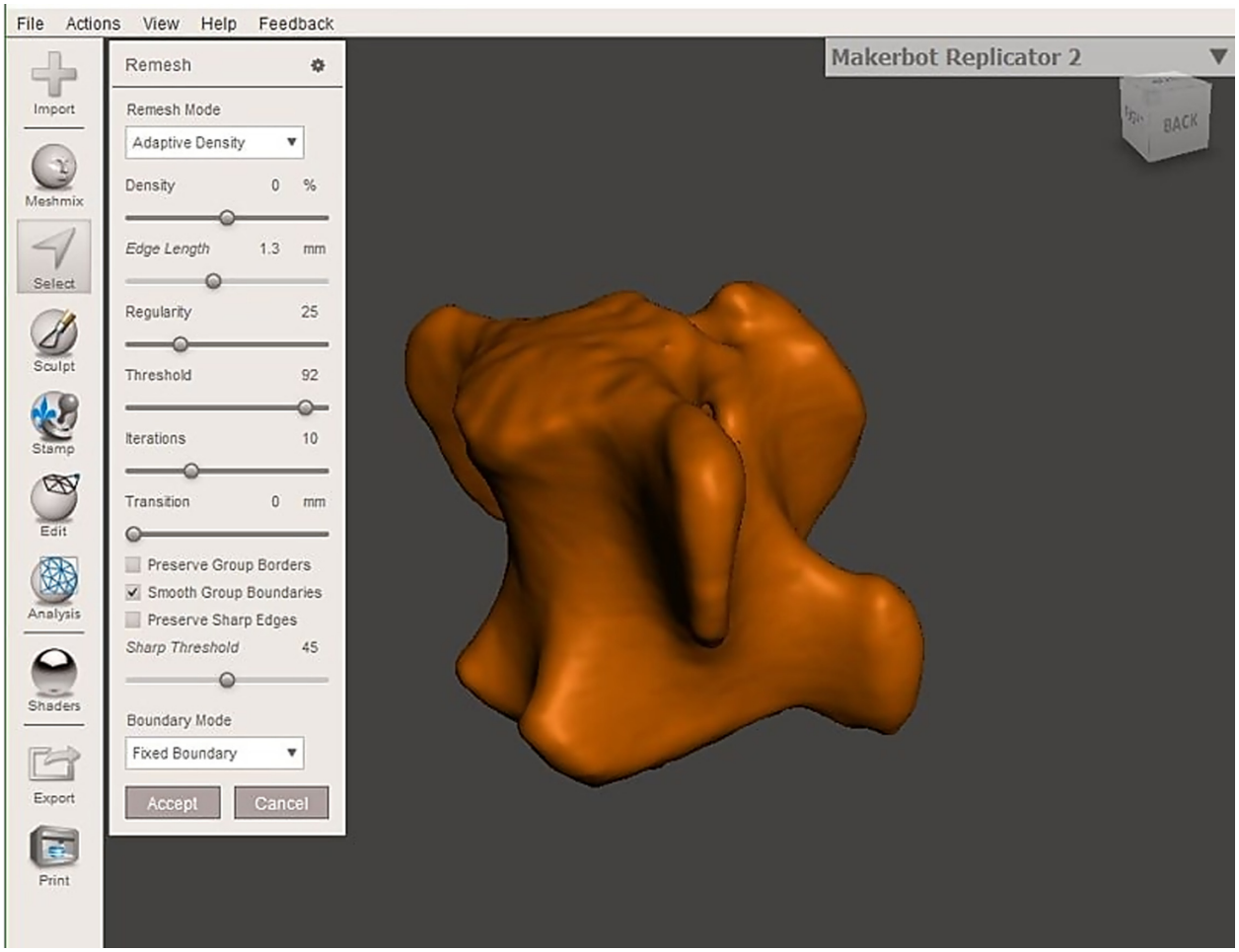

Figure 5. Mesh inspection and repair in Meshmixer version 3.5 (Autodesk inc., San Rafael, CA, USA).[23]

Figure 6. 3D-printed models produced by a Malyan M200 3D printer (Zhangzhou Changfeng Computer Equipment Co., Ltd, China).

measurements. The mean absolute error (and mean relative error) from the original vertebrae and phantom specimen measurements for the 0.1, 0.3, 0.5 and 1 mm 3D-printed models measurements were 0.592 ± 0.396 mm (2.565 ± 2.178%), 0.598 ± 0.479 mm (3.184 ± 5.087%), 0.712 ± 0.498 mm (3.947 ± 5.242%) and 0.933 ± 0.457 mm (4.749 ± 4.701%) respectively.

Approximately half of the 0.3 mm measurements were greater than the corresponding measurement of the 0.1 mm models, whilst approximately half were less, resulting in a comparable mean absolute error. Whilst absolute error and per cent relative error of the 0.5 mm models are higher overall than the 0.1 and 0.3 mm models, several individual measurements of the 0.5 mm model were lower than the corresponding measurements for the 0.1 and 0.3 mm models. The 1 mm model absolute error and per cent relative error was higher than the 0.5 mm in nearly all instances.

The statistical analysis data are summarised in Table 4. All the ICC of parameters were greater than 0.990, indicating that there is little intra-observer variability that is not part of a systematic difference and that the measurements from the original specimens and 3D-printed models can be considered the same for analysis.

Table 1. Dimensional measurements (mm) obtained with digital calipers.

	Linear measurement (mm)				
Model Measurement	Original	0.1 mm SRI	0.3 mm SRI	0.5 mm SRI	1 mm SRI
Phantom 1					
Tier 1 diameter	28.00	28.67	28.01	29.22	29.29
Tier 2 diameter	19.80	20.67	20.23	21.37	21.71
Tier 3 diameter	14.00	14.62	14.36	15.47	15.48
Tier 4 diameter	10.00	10.59	9.90	11.12	11.01
Tier 1 base	15.00	14.99	15.06	15.69	15.73
Phantom height	60.00	59.90	60.00	60.90	60.86
Phantom 2					
Tier 1 diameter	14.00	15.10	15.11	15.23	15.72
Tier 2 diameter	10.00	10.71	10.95	11.37	11.21
Tier 1 height	45.00	45.48	45.65	45.63	45.87
Tier 1 internal diameter	12.00	12.05	12.88	13.21	13.30
Tier 2 internal diameter	5.00	4.97	6.49	6.34	6.20
Phantom height	60.00	60.45	61.59	61.85	61.20
Vertebrae 1					
Left transverse process to right transverse process	68.42	69.45	69.18	69.53	69.86
Left inferior articular facet to right inferior articular facet	34.43	35.45	35.54	35.33	35.26
Left transverse process width	18.65	19.21	19.32	18.95	18.94
Right transverse process width	19.87	20.48	20.40	20.61	20.57
Spinous process length	19.80	21.63	20.57	19.59	20.02
Vertebral body height	40.34	41.38	41.31	41.27	41.91
Left posterior vertebral canal	22.47	23.22	23.44	23.43	23.29
Right posterior vertebral canal	21.42	22.01	22.23	21.68	22.16
Vertebrae 2					
Left transverse process to right transverse process	54.33	54.25	54.36	54.29	54.52
Left inferior articular facet to right inferior articular facet	36.79	37.76	37.08	37.16	37.81
Left transverse process width	19.83	20.01	20.01	19.56	20.27
Right transverse process width	19.44	19.58	19.39	19.93	20.54
Spinous process length	24.76	24.56	24.85	25.05	25.76
Vertebral body height	39.67	40.20	39.69	40.01	40.92
Left posterior vertebral canal height	18.15	18.38	18.27	18.58	18.68
Right posterior vertebral canal height	19.35	19.55	19.36	19.59	19.87
Vertebrae 3					
Left transverse process to right transverse process	42.60	43.21	43.45	43.30	43.51
Anterior-posterior vertebral length	50.13	51.27	51.85	51.35	51.37
Left vertebral body height	24.48	24.96	25.41	24.79	25.88
Right vertebral body height	24.54	25.10	24.23	24.45	25.44
Spinous process length	24.00	24.76	24.81	24.39	25.03
Anterior vertebral body height	24.13	24.68	25.11	24.43	24.62
Left lamina height	23.87	24.92	24.30	23.95	23.86
Right lamina height	24.42	24.93	24.89	24.47	24.60

The paired t-test indicated there was a statistically significant difference between all original specimens and corresponding 3D-printed models except the 0.1 mm vertebrae 2 ($P = 0.097$), the 0.3 mm phantom 1 ($P = 0.209$) and the 0.3 mm vertebrae 2 ($P = 0.061$).

The sizes of the data files are summarised in Table 5. Data sizes ranged from 3.81 MB to 461.01 MB in DICOM format, representing an increase in data size by a factor of ten when decreasing SRI from 1 to 0.1 mm. Data sizes ranged from 1.44 to 31.02 MB in STL format. Increasing the SRI was shown to reduce the digital file sizes of both formats.

Discussion

Measurements demonstrated that changing the SRI of the original specimen scan data sets influenced the spatial replication accuracy of the paired 3D-printed models. Decreasing the SRI was shown to reduce the mean absolute error between comparative measurements of

Table 2. Dimensional virtual measurements (mm) obtained in Meshmixer.

	Linear measurement (mm)			
Model Measurement	0.1 mm SRI	0.3 mm SRI	0.5 mm SRI	1 mm SRI
Phantom 1				
Tier 1 diameter	28.46	28.21	29.25	28.99
Tier 2 diameter	20.62	20.20	21.54	21.76
Tier 3 diameter	14.60	14.46	15.32	15.21
Tier 4 diameter	10.59	9.90	11.01	11.11
Tier 1 base	15.01	15.16	15.70	15.75
Phantom height	59.82	60.10	61.10	60.90
Phantom 2				
Tier 1 diameter	15.31	15.20	15.26	15.75
Tier 2 diameter	10.62	11.11	11.32	11.03
Tier 1 height	45.40	45.79	45.77	45.67
Tier 1 internal diameter	12.15	13.00	13.01	13.32
Tier 2 internal diameter	5.12	6.59	6.28	5.83
Phantom height	60.54	61.60	61.84	60.99
Vertebrae 1				
Left transverse process to right transverse process	69.31	69.31	69.55	70.00
Left inferior articular facet to right inferior articular facet	35.46	35.65	35.34	35.76
Left transverse process width	19.20	19.10	18.65	18.77
Right transverse process width	20.59	20.12	20.65	20.58
Spinous process length	21.60	20.66	19.61	20.02
Vertebral body height	41.31	41.50	41.33	41.90
Left posterior vertebral canal	23.33	23.54	23.55	23.14
Right posterior vertebral canal	22.21	22.83	21.36	22.17
Vertebrae 2				
Left transverse process to right transverse process	54.28	54.36	54.12	54.55
Left inferior articular facet to right inferior articular facet	37.70	37.10	37.18	38.01
Left transverse process width	20.13	20.33	19.57	20.37
Right transverse process width	19.77	19.03	19.99	20.64
Spinous process length	24.95	25.25	25.41	25.32
Vertebral body height	40.28	39.88	40.22	40.90
Left posterior vertebral canal height	18.52	18.26	18.22	18.60
Right posterior vertebral canal height	19.51	19.93	19.63	19.90
Vertebrae 3				
Left transverse process to right transverse process	43.22	43.55	43.35	43.52
Anterior-posterior vertebral length	51.42	51.99	51.35	51.11
Left vertebral body height	25.21	25.42	24.88	26.38
Right vertebral body height	25.19	24.10	24.37	24.94
Spinous process length	24.95	24.60	24.38	25.23
Anterior vertebral body height	24.64	25.02	24.44	24.62
Left lamina height	24.96	24.02	23.99	23.88
Right lamina height	25.22	24.45	24.42	24.70

paired models. However, reducing the SRI below the primary limiting factors does not necessarily improve accuracy, and consequently, the added file size and processing time does not appear to be warranted. This highlights that a benefit may exist in using a smaller SRI, when data size and time invested processing the data are also considered.

In this study, it has been shown that using a SRI significantly smaller than the primary limiting factor of either acquisition slice or printer spatial resolution capabilities potentially results in loss of accuracy due to the sum of processing error, printer error and spatial resolution limitations of the acquisition slice width. This results in the loss of the replication accuracy benefit of the smaller SRI, whilst still experiencing the disadvantage of increased digital size and processing time dealing with the larger data sets. Conversely, using a SRI significantly greater than the primary limiting factor of acquisition slice width or printer spatial resolution capabilities potentially results in loss of accuracy due to the sum of

Table 3. Absolute error (mm) and percentage relative error (%) of model measurement when compared against the corresponding measurement on original specimens.

	Absolute measurement error (mm) (%)			
Model measurement	0.1 mm SRI	0.3 mm SRI	0.5 mm SRI	1 mm SRI
Phantom 1				
Tier 1 diameter	0.67 (2.39%)	0.01 (0.04%)	1.22 (4.36%)	1.29 (4.61%)
Tier 2 diameter	0.87 (4.39%)	0.43 (2.17%)	1.57 (7.93%)	1.91 (9.65%)
Tier 3 diameter	0.62 (4.43%)	0.36 (2.57%)	1.47 (10.50%)	1.48 (10.57%)
Tier 4 diameter	0.59 (5.90%)	0.10 (1.00%)	1.12 (11.20%)	1.01 (10.10%)
Tier 1 base	0.01 (0.07%)	0.06 (0.40%)	0.69 (4.60%)	0.73 (4.87%)
Phantom height	0.10 (0.17%)	0.00 (0.00%)	0.90 (1.50%)	0.86 (1.43%)
Phantom 2				
Tier 1 diameter	1.10 (7.86%)	1.11 (7.93%)	1.23 (8.79%)	1.72 (12.29%)
Tier 2 diameter	0.71 (7.10%)	0.95 (9.50%)	1.37 (13.70%)	1.21 (12.10%)
Tier 1 height	0.48 (1.07%)	0.65 (1.44%)	0.63 (1.40%)	0.87 (1.93%)
Tier 1 internal diameter	0.05 (0.42%)	0.88 (7.33%)	1.21 (10.08%)	1.30 (10.83%)
Tier 2 internal diameter	0.03 (0.60%)	1.49 (29.80%)	1.34 (26.80%)	1.20 (24.00%)
Phantom height	0.45 (0.75%)	1.59 (2.65%)	1.85 (3.08%)	1.20 (2.00%)
Vertebrae 1				
Left transverse process to right transverse process	1.03 (1.51%)	0.76 (1.11%)	1.11 (1.62%)	1.44 (2.10%)
Left inferior articular facet to right inferior articular facet	1.02 (2.96%)	1.11 (3.22%)	0.90 (2.61%)	0.83 (2.41%)
Left transverse process width	0.56 (3.00%)	0.67 (3.59%)	0.30 (1.61%)	0.29 (1.55%)
Right transverse process width	0.61 (3.07%)	0.53 (2.67%)	0.74 (3.72%)	0.70 (3.52%)
Spinous process length	1.83 (9.24%)	0.77 (3.89%)	0.21 (1.06%)	0.22 (1.11%)
Vertebral body height	1.04 (2.58%)	0.97 (2.40%)	0.93 (2.31%)	1.57 (3.89%)
Left posterior vertebral canal height	0.75 (3.34%)	0.97 (4.32%)	0.96 (4.27%)	0.82 (3.65%)
Right posterior vertebral canal height	0.59 (2.75%)	0.81 (3.78%)	0.26 (1.21%)	0.74 (3.45%)
Vertebrae 2				
Left transverse process to right transverse process	0.08 (0.15%)	0.03 (0.06%)	0.04 (0.07%)	0.19 (0.35%)
Left inferior articular facet to right inferior articular facet	0.97 (2.64%)	0.29 (0.79%)	0.37 (1.01%)	1.02 (2.77%)
Left transverse process width	0.18 (0.91%)	0.18 (0.91%)	0.27 (1.36%)	0.44 (2.22%)
Right transverse process width	0.14 (0.72%)	0.05 (0.26%)	0.49 (2.52%)	1.10 (5.66%)
Spinous process length	0.20 (0.81%)	0.09 (0.36%)	0.29 (1.17%)	1.00 (4.04%)
Vertebral body height	0.53 (1.34%)	0.02 (0.05%)	0.34 (0.86%)	1.25 (3.15%)
Left posterior vertebral canal height	0.23 (1.27%)	0.12 (0.66%)	0.43 (2.37%)	0.53 (2.92%)
Right posterior vertebral canal height	0.20 (1.03%)	0.01 (0.05%)	0.24 (1.24%)	0.52 (2.69%)
Vertebrae 3				
Left transverse process to right transverse process	0.61 (1.43%)	0.85 (2.00%)	0.70 (1.64%)	0.91 (2.14%)
Anterior-posterior vertebral length	1.14 (2.27%)	1.72 (3.43%)	1.22 (2.43%)	1.24 (2.47%)
Left vertebral body height	0.48 (1.96%)	0.93 (3.80%)	0.31 (1.27%)	1.40 (5.72%)
Right vertebral body height	0.56 (2.29%)	0.31 (1.26%)	0.09 (0.37%)	0.90 (3.67%)
Spinous process length	0.76 (3.17%)	0.81 (3.37%)	0.39 (1.63%)	1.03 (4.29%)
Anterior vertebral body height	0.55 (2.28%)	0.98 (4.06%)	0.30 (1.24%)	0.49 (2.03%)
Left lamina height	1.05 (4.40%)	0.43 (1.80%)	0.08 (0.34%)	0.01 (0.04%)
Right lamina height	0.51 (2.09%)	0.47 (1.92%)	0.05 (0.20%)	0.18 (0.74%)
Mean of absolute differences	0.592 (2.565%)	0.598 (3.184%)	0.712 (3.947%)	0.933 (4.749%)
SD of absolute differences	0.396 (2.178%)	0.479 (5.087%)	0.498 (5.242%)	0.457 (4.701%)

volume averaging effects, print error, processing error and the loss of spatial resolution that occurs as a result of using a SRI significantly larger than the slice width. Using a SRI similar to the primary limiting factor of acquisition slice width or printer spatial resolution capabilities optimises the replication accuracy of the model whilst minimising the digital size of the data and time investment. These findings will facilitate workflow speed and streamlining and aid in reducing the risk of negative clinical impacts from inaccurate models in surgical applications.[4]

Slice thickness and SRI have been identified by Winder and Bibb (2005, cited by van Eijnatten et al.[5]) as primary limiting factors of replication accuracy from an imaging perspective. Research by McMenamin et al.[6] and Taft et al.[24] identified errors in accuracy of approximately the slice thickness of the respective CT scanner used. This has also been noted in this study, where even the most

Table 4. Mean error, intraclass correlation coefficient (ICC) results and *P*-values (*P*) and t-scores (T) of paired t-tests performed in SPSS version 25.

Analysis	0.1 mm SRI	0.3 mm SRI	0.5 mm SRI	1 mm SRI
Phantom 1				
Mean error (mm)	0.496	0.156	1.112	1.183
T	−2.717	−1.441	−8.519	−6.775
P	0.042	0.209	0.001	0.001
ICC	1.000	1.000	1.000	1.000
Phantom 2				
Mean error (mm)	0.489	1.108	1.222	1.22
T	−2.685	−7.467	−7.958	−11.189
P	0.044	0.001	0.001	0.001
ICC	1.000	1.000	1.000	1.000
Vertebrae 1				
Mean error (mm)	0.948	0.820	0.626	0.796
T	−6.273	−12.536	−3.856	−4.875
P	0.001	0.001	0.006	0.002
ICC	1.000	1.000	1.000	1.000
Vertebrae 2				
Mean error (mm)	0.335	0.095	0.259	0.726
T	−1.913	−2.235	−2.535	−5.607
P	0.097	0.061	0.039	0.001
ICC	1.000	1.000	1.000	1.000
Vertebrae 3				
Mean error (mm)	0.727	0.809	0.342	0.74
T	−7.866	−3.594	−2.488	−4.333
P	0.001	0.009	0.042	0.003
ICC	1.000	0.999	0.999	0.999
Total				
Mean of absolute differences (mm)	0.592	0.598	0.712	0.933
SD of absolute differences (mm)	0.396	0.479	0.498	0.457

Highlighted *P*-values indicate models with non-statistically significant differences, indicating higher spatial replication accuracy.

accurate models contain mean variation of approximately 0.5 mm, equal to the acquisition slice width. However, the spatial resolution error of FDM printers can be significant relative to the acquisition slice width and SRI distances due to printer nozzle width limitations.[10] This is particularly applicable in this study where the FDM printer nozzle width of 0.4 mm is similar to the acquisition slice width of 0.5 mm. Consequently, the exact allocation of error from an imaging or printing standpoint into spatial replication accuracy cannot be ascertained from this study alone. Thus, a single limiting factor cannot be determined with certainty. Consequently, the study may be repeated with a smaller CT slice width or printing technology with a better spatial resolution for further evaluation.

The mean error calculated for the models created from the 0.1 and 0.3 mm SRI data (0.592 and 0.598 mm, respectively) are comparable to other FDM study

Table 5. Data size of digital imaging and communications in medicine (DICOM) and stereolithography (STL) files for each reconstruction file.

	Data Size (MB)			
Data Format	0.1 mm SRI	0.3 mm SRI	0.5 mm SRI	1 mm SRI
Phantom 1				
DICOM	24.53	18.76	11.35	5.81
STL	31.02	14.34	8.54	4.42
Phantom 2				
DICOM	24.53	18.78	11.39	5.83
STL	22.46	8.84	5.31	3.22
Vertebrae 1				
DICOM	35.44	11.89	7.16	3.81
STL	10.28	3.36	3.35	1.95
Vertebrae 2				
DICOM	252.2	84.93	51.14	25.86
STL	6.22	3.26	2.23	1.44
Vertebrae 3				
DICOM	461.01	153.98	92.68	46.55
STL	13.64	6.45	4.34	2.45

measurements that are commonly accepted as suitable for surgery, such as the mean error of 0.56 mm of a FDM model analysed by Petropolis et al.[12] The mean error in the models within this study is similar to or less than the reported mean errors for specimens produced by other expensive 3D printing technologies. Salmi et al.[19] noted a mean error in selective layer sintering models of 0.79 and 0.80 mm, whilst McMenamin et al.[6] identified a mean error of 0.53 mm in a material jetting model. Some substantial replication error has been noted in previous studies, as indicated by the measurement error ranging from 0.8 to 1.5 mm noted in models analysed by Ogden et al.[20]

The variation in the digital size of the data sets highlights the balance of data volume with anatomical detail and image resolution, which is important where storage space and long-term archiving are considered.[8] Smaller slice widths are associated with larger data sets due to an increased number of slices.[8] Similarly, this study highlighted that with decrease in SRI there was an approximately proportional increase in STL file size, with a proportional increase in the number of slices in each data set.

Limitations

The production of 3D-printed models from CT scan data involves a large parameter variability space that can permit the introduction of bias and error at all stages, particularly where multiple software programs are used.[1,5,9,20] Evaluation of the factors that influence spatial

replication accuracy at each of these steps is vital to appreciating and further refining this technology, and to provide greater context in which to understand these results, particularly as a combination of these factors may play a role in accuracy variance between models of both varying and equal SRIs.[1,10]

Segmentation

Poor segmentation can be a significant source of error introduction, and the choice of automatic threshold value and technique of manual segmentation to isolate anatomy have all been proven to have an effect on replication accuracy.[5,13,20] George et al.[10] have indicated that poor segmentation can introduce error reaching up to 4 mm. To minimise error introduction, dried bovine vertebrae free of soft tissue and a forearm phantom surrounded by water-equivalent resin were used to simplify the segmentation process.

Triangulation

The algorithmic aspect of translating the segmented data into an STL model can adversely affect model replication accuracy.[10,20] To minimise introducing additional error, the triangulation in this study was performed at the highest resolution offered by 3D Slicer. However, even high-resolution triangulation techniques can still digitally alter the model by over-smoothing surfaces.

Printing

Models printed by FDM may exhibit warping or deformation and may become brittle over extended periods of time.[10] Contact with liquids or exposure to high humidity can accelerate this process.[10] In this study, models were measured within a week of construction and kept clear of any sources of damage to minimise error introduction. However, the addition and subsequent removal of support structures required during printing may have also introduced minimal error.[10,20]

Measurement

There is no gold standard for the measurement of replication accuracy in medical 3D printing applications.[1,12,19,25] The use of calipers to physically measure designated anatomical measurements is one of the most common methods of determining the spatial replication accuracy of these models.[1,6,12,13,20,25] However, this method may introduce potential measurement error. The ability to locate the exact same landmarks precisely is limited, which may introduce some artificial variability. This issue was magnified when utilising digital measurements in Meshmixer due to the difficulty placing the cursor on the exact selected landmark. Furthermore, the original specimens were unable to measure digitally prior to the introduction of CT spatial resolution error that occurs as a result of 0.5 mm slice width limitations, and thus, digital measurements were not used for the purpose of statistical analysis.

Conclusion

There is currently limited literature on the impact of CT scan reconstruction parameters on the spatial replication accuracy of 3D-printed anatomical models. This study has successfully achieved research aims by demonstrating that changing the SRI influences the spatial replication accuracy of 3D-printed anatomical models. It has also demonstrated that a benefit exists in using a SRI equal to or less than the primary limiting factor of either the acquisition slice width or printer capabilities by optimising the replication accuracy of the model whilst minimising the digital size of the data and required processing time investment. Consequently, this study can help refine 3D printing protocols in medical and tissue engineering applications and help practitioners to create accurate reproductions of anatomy for various teaching and clinical purposes.

Conflicts of Interest

The authors declare no conflicts of interest.

Acknowledgements

Access to the equipment and resources of the Queensland University of Technology Medical Engineering Research Facility is greatly appreciated.

References

1. Odeh M, Levin D, Inziello J, et al. Methods for verification of 3D printed anatomic model accuracy using cardiac models as an example. 3D Printing In. *Medicine* 2019; **5**: 6.
2. Sun Z. Insights into 3D printing in medical applications. *Quant Imaging Med Surg* 2019; **9**: 1–5.
3. Osti F, Santi GM, Neri M, et al. CT conversion workflow for intraoperative usage of bony models: From DICOM data to 3D printed models. *Applied Sciences* 2019; **9**: 708.
4. Foo GL, Kwek EBK. Are three-dimensional printed models useful for preoperative planning of tibial plafond fractures? *J Foot Ankle Surg* 2019; **58**(4): 723–729.
5. van Eijnatten M, van Dijk R, Dobbe J, Streekstra G, Koivisto J, Wolff J. CT image segmentation methods for bone used in medical additive manufacturing. *Med Eng Phys* 2018; **51**: 6–16.

6. McMenamin PG, Quayle MR, McHenry CR, Adams JW. The production of anatomical teaching resources using three-dimensional (3D) printing technology. *Anatomical Sciences Education* 2014; **7**: 479–86.
7. Ahangar P, Cooke ME, Weber MH, Rosenzweig DH. Current biomedical applications of 3D printing and additive manufacturing. *Appl Sci* 2019; **9**: 1713.
8. Ford JM, Decker SJ. Computed tomography slice thickness and its effects on three-dimensional reconstruction of anatomical structures. *JOFRI* 2016; **4**: 43–6.
9. Allan A, Kealley C, Squelch A, Wong YH, Yeong CH, Sun Z. Patient-specific 3D printed model of biliary ducts with congenital cyst. *Quant Imaging Med Surg* 2019; **9**: 86.
10. George E, Liacouras P, Rybicki FJ, Mitsouras D. Measuring and establishing the accuracy and reproducibility of 3D printed medical models. *Radiographics* 2017; **37**: 1424–1450.
11. Martelli N, Serrano C, Van Den Brink H, et al. Advantages and disadvantages of 3-dimensional printing in surgery: A systematic review. *Surgery* 2016; **159**: 1485–500.
12. Petropolis C, Kozan D, Sigurdson L. Accuracy of medical models made by consumer-grade fused deposition modelling printers. *Plast Surg (Oakv)* 2015; **23**: 91–4.
13. Bortolotto C, Eshja E, Peroni C, Orlandi MA, Bizzotto N, Poggi P. 3D printing of CT dataset: Validation of an open source and consumer-available workflow. *J Digit Imaging* 2016; **29**: 14–21.
14. Garcia J, Yang Z, Mongrain R, Leask RL, Lachapelle K. 3D printing materials and their use in medical education: A review of current technology and trends for the future. *BMJ Simul Technol Enhanc Learn* 2018; **4**: 27–40.
15. Boone J, Brink J, Edyvean S, et al. Basics of computed-tomography technology. *J ICRU* 2012; **12**: 13–23.
16. Primo BT, Presotto AC, De Oliveira HW, et al. Accuracy assessment of prototypes produced using multi-slice and cone-beam computed tomography. *Int J Oral Maxillofac Surg* 2012; **41**: 1291–5.
17. Dewey M Cardiac CT, 2nd edn. Springer, Berlin Heidelberg; 2014.
18. Huotilainen E, Paloheimo M, Salmi M, et al. Imaging requirements for medical applications of additive manufacturing. *Acta Radiol* 2014; **55**: 78–85.
19. Salmi M, Paloheimo K, Tuomi J, Wolff J, Mäkitie A. Accuracy of medical models made by additive manufacturing (rapid manufacturing). *J Cranio-Maxillofac Surg* 2013; **41**: 603–9.
20. Ogden KM, Aslan C, Ordway N, Diallo D, Tillapaugh-Fay G, Soman P. Factors affecting dimensional accuracy of 3-D printed anatomical structures derived from CT data. *J Digit Imaging* 2015; **28**: 654–63.
21. Queensland Government. Animal Care and Protection Act 2001. Office of Queensland Parliamentary Counsel, Brisbane, 2013.
22. Fedorov A, Beichel R, Kalpathy-Cramer J, et al. 3D Slicer as an image computing platform for the Quantitative Imaging Network. *Magn Reson Imaging* 2012; **30**: 1323–41.
23. MESHMIXER. 3.5 ed. Autodesk, San Rafael, California; 2018.
24. Taft RM, Kondor S, Grant GT. Accuracy of rapid prototype models for head and neck reconstruction. *J Prosthet Dent* 2011; **106**: 399–408.
25. Larguier L, Hespel A-M, Jamet N, et al. Accuracy and precision of measurements performed on three-dimensional printed pelvises when compared to computed tomography measurements. *J Vet Sci* 2019; **20**.